JOURNAL OF PROPULSION AND POWER
Vol. 13, No. 2, March–April 1997

Normal, Sonic Helium Injection Through a Wedge-Shaped Orifice into Supersonic Flow

Matthew J. Barber*
France Compressor Products, Newtown, Pennsylvania 18940
Joseph A. Schetz†
Virginia Polytechnic Institute and State University, Blacksburg, Virginia 24061
and
Larry A. Roe‡
University of Arkansas, Fayetteville, Arkansas 72701

Helium was injected normally to a Mach 3 airstream to simulate hydrogen fuel injection in a scramjet combustor. Two geometries were evaluated, a wedge-shaped wall orifice and a circular wall orifice. Injection was sonic in both geometries, and the expansion ratios and mass flow rates were matched to isolate the effects of the geometric difference. Surface oil flow patterns were inspected to determine the extent of boundary-layer separation upstream of each injector, shadowgraphs were used to visualize the flowfields, and probe measurements were utilized to determine local helium concentrations. The wedge-shaped injection scheme demonstrated more rapid penetration into the freestream and increased mixing when compared to the baseline circular orifice. In addition, the oil flow photography showed that the wedge-shaped injector had no upstream separation zone, whereas the circular injector had a large separation zone. The wedge configuration would therefore be expected to exhibit reduced wall heat transfer in an actual combustor. It is concluded that wedge-shaped, normal, fuel injectors should provide generally better performance than circular normal injectors in supersonic combustors.

Nomenclature

A = jet cross-sectional area
h = penetration distance
M = Mach number
$\dot{m}$ = mass flow rate
R_b = nondimensionalization parameter
u = flow velocity
x = axial distance downstream of injector
y = lateral distance from the injector centerline
z = vertical distance from wind-tunnel floor
α_{He} = helium mass fraction
β_1 = regression constant
β_2 = regression constant
η_1 = penetration rate
η_2 = decay rate of helium mass fraction
η_3 = area growth rate of jet
ρ = density

Subscripts
j = jet property
∞ = freestream property

Introduction

COMBUSTION processes associated with scramjet engines are of continuing interest to the international propulsion community. Fuel–air mixing in the combustor section is a major component of scramjet research because the fuel and air must mix and react with residence times on the order of a millisecond to produce acceptable thrust levels. The performance of the combustor and the overall performance of the engine depend on how adequately mixing and combustion occur. Therefore, any improvement in mixing will result in a better engine with increased thrust. Additionally, most fuel injection schemes provide sufficient blockage to the main flow to produce significant shock and/or separation structures that can greatly increase undesirable heat transfer to the combustor walls. Injection geometries that provide good levels of mixing with minimal flow separation and thermal impact on the injection surface are especially beneficial.

Numerous fuel injection schemes have been investigated. Typical methods include axial injection through steps in the combustor wall, transverse or angled injection through wall orifices, and injection through ramps or behind pylons. Thomas et al.[1] summarize results through 1989 and provide a review of the available high-speed mixing database. A further review is provided by Bogdanoff.[2] One fuel injection technique that has received a significant and continuing amount of study is transverse wall injection.[3–12] For some applications, transverse fuel injection through nonintrusive wall ports may be the optimal choice, even though the mixing performance may not be superior to other injection schemes.

The purpose of the present research, which was initially inspired by the work of Masyakin and Polyanskii,[13] is to investigate simulated fuel injection through a wedge-shaped orifice acting as a transverse wall injector. The objective of the work done by Masyakin and Polyanskii[13] was to determine an injector exit shape such that no three-dimensional boundary-layer separation zone occurred upstream of the injection point. Such a separation zone causes increased pressure and extreme local heat fluxes to the wall, and normal circular injectors have a relatively large separation zone. For normal sonic injection, Masyakin and Polyanskii[13] found that a triangular injector oriented with its apex toward the oncoming flow, and with an apex half-angle less than 12 deg, has no upstream separation

Presented as Paper 95-2559 at the AIAA/ASME/SAE/ASEE 31st Joint Propulsion Conference, San Diego, CA, July 10–12, 1995; received July 19, 1995; revision received July 24, 1996; accepted for publication Aug. 2, 1996.

*Engineer, 104 Pheasant Run.
†W. Martin Johnson Professor, Aerospace and Ocean Engineering Department. Fellow AIAA.
‡Assistant Professor, Mechanical Engineering Department. Senior Member AIAA.

zone. Furthermore, it was found that the absence of the separation zone leads to a change in the system of shock waves upstream of the jet, with no normal shocks being apparent. Based on these results, transverse fuel injection through a properly shaped orifice could potentially result in better fuel mixing than through a circular orifice, whereas the absence of an upstream separation zone should significantly reduce local thermal loading to the combustor walls.

The present research extends the work of Masyakin and Polyanskii[13] by evaluating the mixing achieved when a simulated fuel is injected normally to a Mach 3 airstream through a wedge-shaped injector with its apex oriented toward the oncoming flow. In this study, a wedge shape was used instead of the triangular shape of the prior research primarily because of fabrication considerations. To provide a baseline for comparison, tests were also performed on a single, circular, sonic injector. These tests were under cold-flow conditions, utilizing helium to simulate hydrogen injection.

Experimental Apparatus and Methods

Facilities and Experimental Models

The data for this study were obtained in the 23 × 23 cm blowdown supersonic wind tunnel at Virginia Polytechnic Institute and State University (Fig. 1) at a freestream Mach number of 3.0, freestream total pressure of 6.5 atm, and freestream total temperature of 294 K. This tunnel (described in more detail in Ref. 14) provides run durations of about 13 s under these conditions. The resulting freestream Reynolds number is 5.4×10^5/cm. The test section is 11.4 cm high, 22.8 cm wide, and more than 30 cm long in the streamwise direction, dimensions comparable to an actual scramjet combustor.

The wind tunnel is computer operated and controlled, resulting in accurate and repeatable runs. The total pressure is maintained within ±0.03 atm from run to run, whereas helium pressure is controlled to within 3% of the desired value. The computer system also controls a 12-bit A/D data acquisition system to sample and record various test parameters.

The experimental models consisted of an injector block with two interchangeable injector inserts. Both injectors were sonic and injected helium normal to the main flow. The wedge-shaped injector is shown in Fig. 2. This injector had a wedge length of 10.8 mm and half-angle of 7.35 deg and was situated so that its apex was oriented into the Mach 3 freestream. The circular injector insert incorporated a 3.45-mm-diam hole centered at the same coordinates as the centroid of the wedge-shaped injector. This diameter was chosen to duplicate the flow rate and expansion ratio of the wedge injector. The injector block with insert was mounted on top of a helium plenum chamber, forming a smooth wall along the bottom of the tunnel.

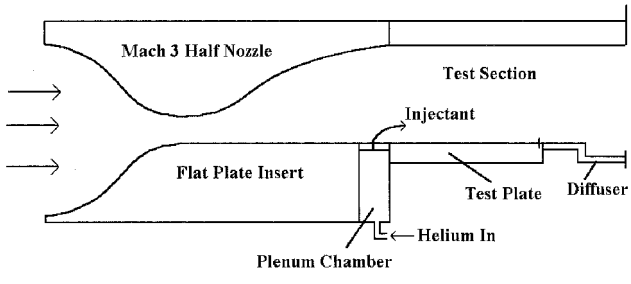

Fig. 1 Tunnel cross section.

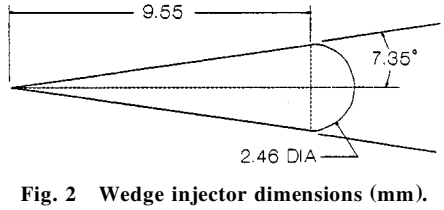

Fig. 2 Wedge injector dimensions (mm).

Since the shape of the injectors was the primary parameter of investigation, the geometric diameter (or equivalent diameter in the case of the wedge-shaped injector) was not a relevant scale for nondimensionalizing the experimental results. Therefore, the effective radius (R_b), as defined by Schetz,[15] was used to reflect the matched flow conditions of the wedge-shaped injector and the circular injector. R_b is defined only in terms of flow parameters and is the approximate nose radius of a solid body used to represent the obstruction to the freestream created by the injected helium and is independent of injector size.[15] All distances were nondimensionalized by R_b, which was determined from the injected helium mass flow rate and freestream conditions:

$$R_b = \sqrt{\dot{m}_j/\rho_\infty u_\infty}$$

Since the injectant mass flow and freestream conditions were the same for both injection geometries, R_b had a value of 1.56 mm for both injectors. Jet total pressure was 75.8 kPa for the wedge-shaped injector and 120 kPa for the circular injector. Other flow conditions were matched. The expansion ratio, defined as the ratio of jet static pressure to the minimum static pressure required to choke the injector, was 1.45, the mass flow rate of helium was 8.9×10^{-4} kg/s, the discharge coefficient was 0.90, and the injected helium had a total temperature of 299 K.

Mean Flow Instrumentation

The local helium concentration was measured with the aspirating hot-film probe developed by Ng et al.[16] for measuring local mean gas composition in supersonic flows. This probe was designed to ensure the swallowing of the standoff shock, which is required for accurate, isokinetic sampling. The swallowing of the shock has been verified by schlieren photographs taken of the probe tip during nominal operating conditions of the tunnel.

Measurements of pitot pressure, cone-static pressure, and total temperature were made by probing the flow. The cone-static probe consisted of a 10-deg semivertex-angle cone with a base diameter of 1.6 mm, whereas a ceramic-tipped, vented, diffuser-type thermocouple probe was used to measure the total temperature. The sampling area of these probes is about 1 × 1 mm.

The reduction of the raw data measured from a pitot probe and a cone-static probe requires knowledge of the local helium concentration to determine the gas constant and specific heat ratio. This information is then used in the Rayleigh–pitot formula and the cone-flow solution to determine the Mach number and the static pressure in the flowfield. Together with the measurements from the total temperature probe, all mean flow quantities such as velocity, density, and local mass flux can thus be calculated. Further details are provided by Ng et al.[16]

Optical Instrumentation

Nanopulse (30×10^{-9} s) shadowgraphs of the flowfield were made for both injection geometries. Features of interest include the thickness of the preinjection boundary layer, shock structure in the injection region, and the downstream development of the mixing and boundary layers.

Surface flow visualization was accomplished using the oil flow method. Drops of oil containing orange or green fluorescent dye were placed on the surface of the injector block upstream and downstream of the injector. During tunnel operation, developing surface oil flow patterns highlighted the separation zones. Ultraviolet lamps enhanced the appearance of the oil for posttest photography.

Experimental Methods and Data Analysis

A test plate downstream of the injector and flush with the tunnel floor contained instrumentation ports that allowed lat-

eral and vertical positioning of mean flow probes. Continuous vertical profiles of helium concentration, pitot pressure, cone-static pressure, and total temperature were obtained at axial stations 56, 97, and 201R_b (8.74, 15.1, and 31.4 cm, respectively) downstream of the injection point. These profiles were taken at the tunnel centerline and at three lateral stations on each side of the centerline. At the third axial location, profiles were also taken at a fourth lateral station on each side of the centerline. Helium concentration, total pressure, static pressure, total temperature, static temperature, Mach number, local speed of sound, density, flow velocity, and mass flux were calculated from the acquired data. The analysis techniques include the examination of oil-flow photographs and composite shadowgraphs, and the determination of concentration-based results such as helium penetration into the main airflow, jet area growth, and downstream decay of the local maximum helium concentration. An uncertainty analysis indicates that the maximum error in local helium concentration is 5%.

Results

Flowfield Visualizations

Figure 3 shows the surface oil flow photographs for both injectors. The oil flow for the circular injector shows a well-defined boundary-layer separation zone upstream of the jet, whereas the oil flow for the wedge-shaped injector shows little or no upstream separation. The downstream wake is seen to be about the same size in both cases.

Visual evaluations of the flowfield shadowgraphs for the circular injector show that the helium first penetrates the freestream slightly at approximately $x/R_b = 51$. By $x/R_b = 74$, the helium penetration extends well above the boundary layer and forms a visible mixing region between the boundary layer and the unmixed air of the freestream. By $x/R_b = 97$, the mixing region has penetrated $8.3R_b$ into the freestream, and at $x/R_b = 201$, penetration is $9.6R_b$. The helium–air mixing layer penetration increases 16% between $x/R_b = 97$ and 201.

For the wedge-shaped injector, the shadowgraphs show that the helium begins to penetrate above the boundary layer at approximately $x/R_b = 45$ and remains above it. By $x/R_b = 56$, penetration into the freestream is $6.4R_b$; at $x/R_b = 97$, penetration is $8.3R_b$; and by $x/R_b = 201$, the mixing region penetrates $12R_b$ into the freestream. The mixing region penetration increases 47% between $x/R_b = 97$ and 201.

A comparison of these data shows increased penetration for the jet issuing from the wedge injector and a higher penetration gradient even at the farthest downstream distances evaluated. At the last station, $x/R_b = 201$, the mixing layer for the wedge-shaped injector penetrates 27% farther into the freestream than the mixing layer for the circular injector.

Concentration Data

Flowfield Structure

Helium concentration data are presented in the form of helium mass fraction contour plots in Figs. 4–9. The plots extend laterally $6R_b$ on either side of the injector centerline for the first two axial stations and $8R_b$ for the third axial station. The figures indicate the numerical magnitude of the maximum helium mass fraction α_{max}, and identify the location of this local maximum with an ×. The minimum contour line ($\alpha = 0.003$) represents the approximate lean limit mass fraction for homogeneous H_2–air deflagration at STP. The ● symbol marks the centroid of the area bounded by this lean-limit contour. The contour lines then proceed at regular intervals of 0.01 helium mass fraction for the first two axial stations and 0.005 helium mass fraction for the third axial station.

Figs. 4–6 are the contour plots for the circular injector. At the first axial station ($x/R_b = 56$, Fig. 4), the core of the jet, as defined by the location of the maximum helium mass fraction, is above the injector centerline at an elevation of $z/R_b = 3.4$. By the second axial station ($x/R_b = 97$, Fig. 5), the core remains along the injector centerline, but is seen to begin dividing into

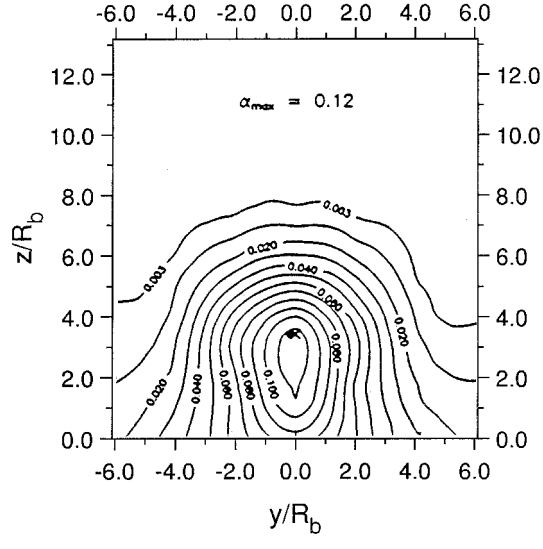

Fig. 4 Helium concentration, circular injector, $x/R_b = 56$.

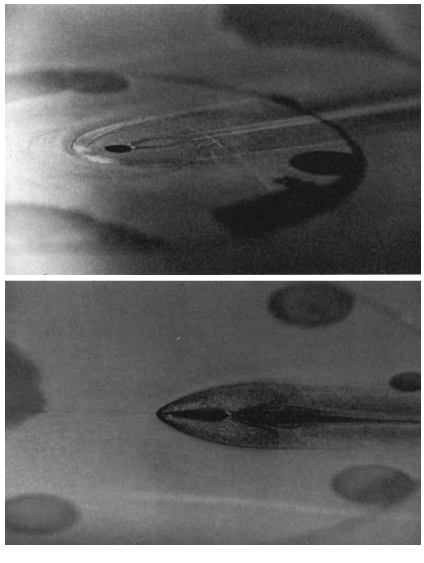

Fig. 3 Surface flow patterns, both injectors.

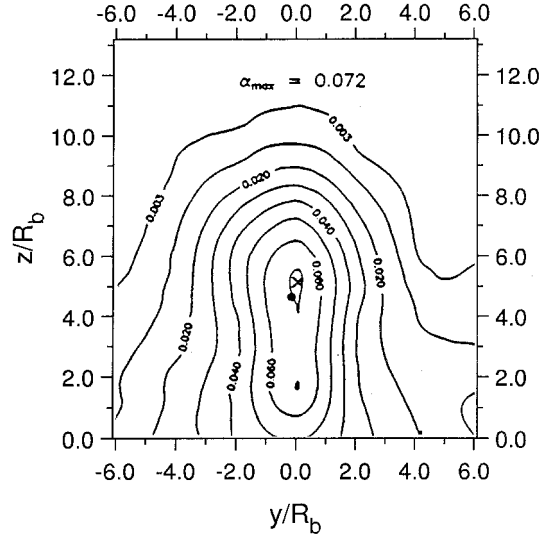

Fig. 5 Helium concentration, circular injector, $x/R_b = 97$.

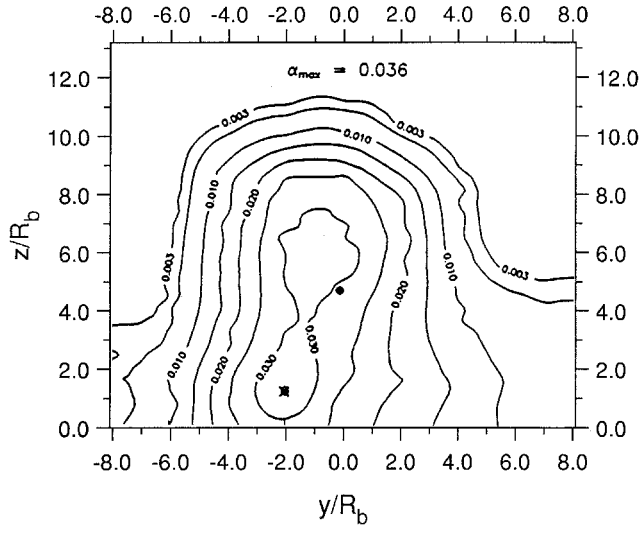

Fig. 6 Helium concentration, circular injector, $x/R_b = 201$.

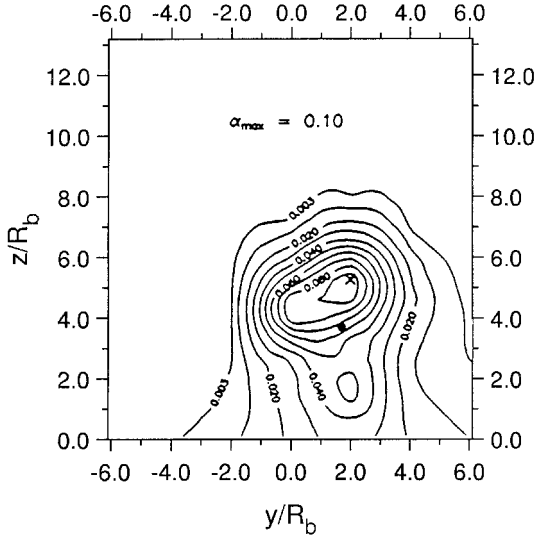

Fig. 7 Helium concentration, wedge injector, $x/R_b = 56$.

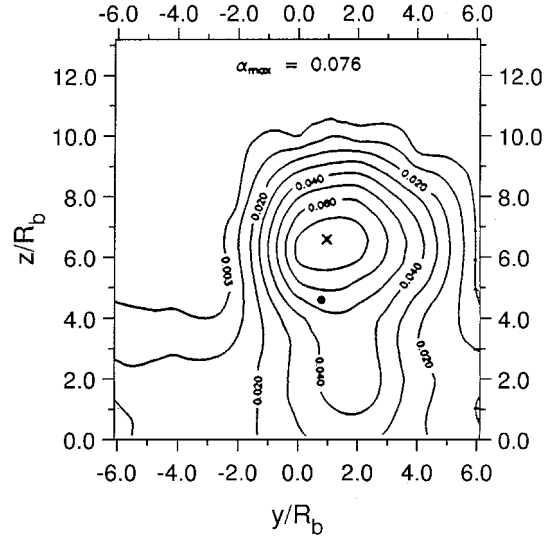

Fig. 8 Helium concentration, wedge injector, $x/R_b = 97$.

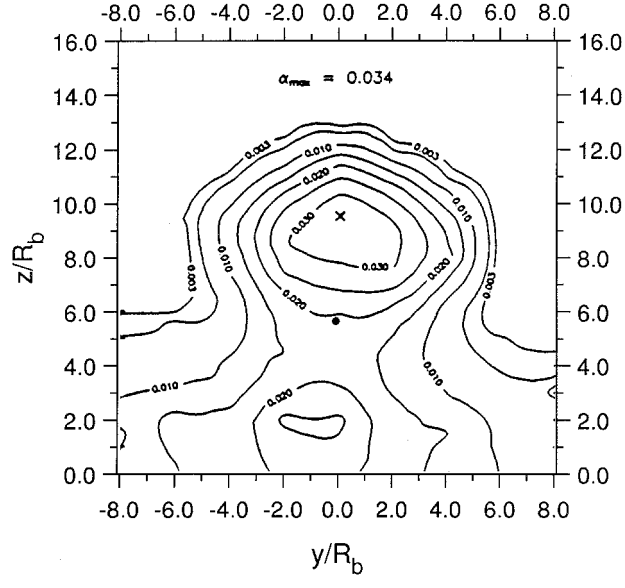

Fig. 9 Helium concentration, wedge injector, $x/R_b = 201$.

two regions, a large one above the boundary layer centered at about $z/R_b = 5.2$ and a much smaller one within the boundary layer, centered at approximately $z/R_b = 1.7$. (At this axial location, the boundary-layer thickness is approximately $3.2R_b$ as shown by the shadowgraphs.)

The contour plot at $x/R_b = 201$ (Fig. 6) shows that the two core regions continue to divide and grow. The lateral position of the core region within the boundary layer has drifted away from the injector centerline to $y/R_b = 2.0$ (indicating a slightly nonsymmetric tunnel condition), whereas the core region above the boundary layer remains along the injector centerline. The vertical positions of the two core centers are approximately $z/R_b = 1.2$ and 5.8.

Contour plots for the wedge-shaped injector can be seen in Figs. 7–9. At the first station, $x/R_b = 56$, the core of the jet is located at approximately $y/R_b = 2.0$ and $z/R_b = 5.2$. By $x/R_b = 97$, as shown in Fig. 8, the core has moved toward the injector centerline and is centered at $y/R_b = 1.0$ and $z/R_b = 6.7$. Figure 9 shows that the core region at $x/R_b = 201$ lies along the injector centerline at $z/R_b = 9.5$. The core region does not bifurcate as rapidly as for the circular injector, but there is an indication of a smaller core region within the boundary layer in Fig. 9.

Penetration Analyses

Three different metrics for jet penetration have been considered and are plotted in Fig. 10. The penetration of the core center (point of maximum concentration, marked by an × in the previous contour plots) is plotted as a function of axial distance, where h_{core} is the elevation of the core center above the tunnel floor. These data have been characterized by a logarithmic equation of the form:

$$h_{core}/R_b = \eta_1 \log(x/R_b) + \beta_1$$

where the constants η_1 and β_1 are determined by linear regression. The rate of penetration of the core center is represented by η_1.

For the circular injector, the data represent that portion of the core that penetrates into the freestream and neglects the region remaining within the boundary layer. The rate of core center penetration is $\eta_1 = 4.1$. The core center penetration for the wedge-shaped injector is also shown in Fig. 10, along with the results of the curve fit. The penetration rate is $\eta_1 = 7.8$, 89% greater than the rate for the circular injector. The absolute value of the core center penetration for the wedge-shaped injector is 53% greater than the value for the circular injector at $x/R_b = 56$, and 64% greater at $x/R_b = 201$.

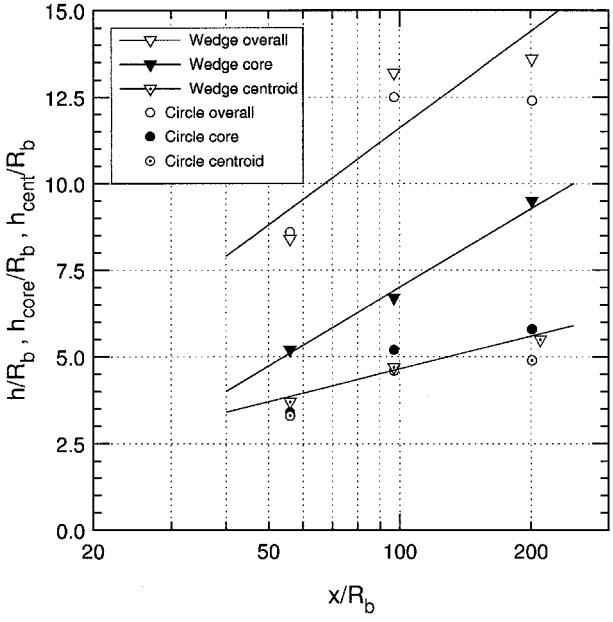

Fig. 10 Helium penetration into Mach 3 stream.

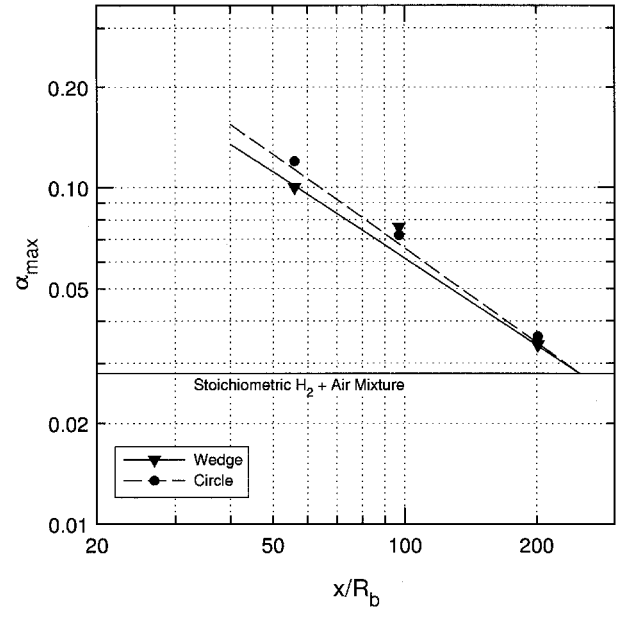

Fig. 11 Decay of maximum helium concentration.

The location of the centroid of the region bounded by the H_2–air deflagration lean limit is also plotted in Fig. 10. These data have also been fit to a logarithmic form, but with η_1 representing the rate of penetration of the centroid of the jet. The jet from the circular injector has a rate of centroid penetration of $\eta_1 = 2.4$; the centroid penetration rate for the jet from the wedge-shaped injector is $\eta_1 = 3.2$, 31% greater than that of the circular injector. At $x/R_b = 56$, the centroid of the jet from the wedge-shaped injector shows 8.7% greater penetration than the centroid of the jet from the circular injector, and by $x/R_b = 201$ the advantage has increased to 14%.

Also indicated in Fig. 10 is the overall penetration at each axial station. The overall penetration is defined, in this case, as the minimum value of z/R_b, along the injector centerline ($y/R_b = 0.0$), which has a helium mass fraction less than 7.0×10^{-4}. This definition is consistent with that used by Rogers.[3] The difficulty of locating this low-concentration point (within the experimental uncertainty) limits the usefulness of this form of data presentation, however, results are included for completeness and reference to other studies. The data again fit a logarithmic equation, with η_1 in this case representing the rate of overall penetration of the jet. The penetration rate for the jet from the circular injector is $\eta_1 = 6.5$, while the penetration rate for the jet from the wedge-shaped injector is $\eta_1 = 9.2$, an improvement of 42%. The overall penetration of the jet from the wedge-shaped injector is 4.2% less than the overall penetration of the jet from the circular injector at $x/R_b = 56$, but is 9.4% greater at $x/R_b = 201$.

Decay of Maximum Local Helium Concentration

Penetration analyses, while frequently utilized in the past for jet studies, do not totally reflect the mixing processes that are occurring. Figure 11 shows the variation of maximum helium concentration with axial distance for both injectors. This provides a different type of assessment, since the local maximum helium concentration will, in general, decrease with distance downstream because of mixing between the helium and air, whereas penetration can occur even in the absence of mixing. The following relation was used to compare the data:

$$\alpha_{max} = \beta_2 (x/R_b)^{-\eta_2}$$

where β_2 and η_2 were determined from a least-square fit to the data. The exponent η_2 represents the helium–air mixing rate. The stoichiometric hydrogen–air concentration line is shown for reference.

The decay rates and intersections with the stoichiometric line are essentially the same for both injectors. The rate of maximum helium concentration decay for the jet from the wedge-shaped injector is $\eta_2 = 0.86$, which is 6.6% less than for the jet from the circular injector, $\eta_2 = 0.92$. If the decay rates were to remain constant beyond $x/R_b = 201$, as drawn, the distance required for the maximum local concentration to fall to the H_2–air stoichiometric line would be $260R_b$ for the jet from the circular injector, whereas the distance for the jet from the wedge-shaped injector would be $262R_b$, which is the same, within the experimental uncertainty of the data.

The maximum helium concentration for injection from the wedge-shaped injector is 14% lower than that for the circular injector at $x/R_b = 56$ and 5.6% lower at $x/R_b = 201$.

Jet Cross-Sectional Area

The growth of jet cross-sectional area (represented as the region bounded within the homogeneous H_2–air deflagration lean limit contour) is shown in Fig. 12. The area has been nondimensionalized by R_b^2. These data have again been fitted

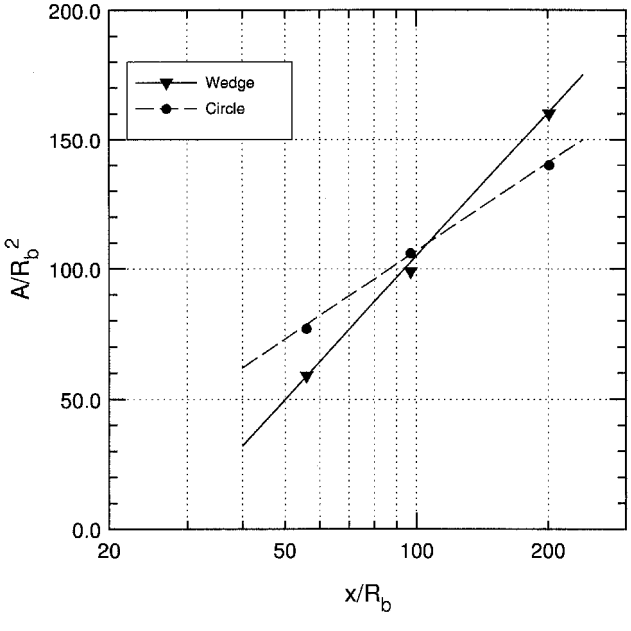

Fig. 12 Growth of jet cross-sectional area.

to a logarithmic function with jet cross-sectional growth indicated by the coefficient η_3.

The rate of area growth is a good indication of jet expansion in both the lateral and vertical directions. The rate of area growth is $\eta_3 = 112$ for the circular case and $\eta_3 = 182$ for the wedge-shaped case, a difference of 63%. At the first axial station, $x/R_b = 56$, the area of the jet from the wedge-shaped injector is 24% less than the area of the jet from the circular injector. However, by $x/R_b = 201$, the area of the jet from the wedge-shaped injector has increased to be 14% greater than that of the jet from the circular injector.

Discussion

The weight of the experimental evidence supports improved mixing for the wedge-shaped injector. Since the two injectors have the same expansion ratio and mass flow, variations in the mixing characteristics are concluded to result from geometric differences only. The geometric differences cause changes in the near flowfield and system of shock waves upstream of the injectors, which lead to differences in the upstream boundary-layer separation zones.[13] Although the shadowgraphs indicate that both jet shock waves are of equivalent strengths, surface oil flow patterns show that the wedge-shaped injector has no discernible upstream boundary-layer separation zone. The absence of a separation zone indicates that the shock wave system for the wedge-shaped injector differs from that of the circular injector, although the differences are not readily apparent from the shadowgraphs.

Both jets develop bifurcated cores, with one core region penetrating the freestream and another core remaining within the boundary layer. The core of the jet from the circular injector begins dividing by the second axial station, and the core of the jet from the wedge-shaped injector by the third axial station. The core division is apparently a result of reduced near-wall mixing caused by low velocities within the boundary layer.

To compare the injectors, parameters describing mixing performance were calculated. Based on the degree of confidence in the data measurements, the primary comparison parameters include the maximum helium concentration decay rate and the growth of jet cross-sectional area. Of the three penetration parameters (core center, overall, and centroid), centroid penetration is felt to provide the most meaningful data interpretation, although all penetration-type evaluations have inherent weaknesses.

The maximum concentration decay rate, the most frequently used basis of comparison for gas mixing in the near-injection region, is the rate at which the local maximum helium mass fraction decays with axial distance. A high decay rate indicates a large amount of mixing between the injected helium and the air. The decay rate for the wedge-shaped injector is 6.6% less than the decay rate for the circular injector. This (alone among the comparison techniques) indicates slightly superior mixing performance for the circular injector.

Another comparison method related to decay rate is the mixing distance, defined as the axial position at which the maximum local fuel concentration reaches the stoichiometric value. The mixing distances for both injectors are the same, indicating that circular injectors in a combustor design could be replaced with matched wedge-shaped injectors without increasing combustor length.

Overall penetration is a measure of how far the outer regions of the fuel jet move into the freestream. Overall penetration is (typically) based on very low values of α, near the limits of the instrument resolution and within a range of low signal-to-noise ratio. This generates a significant uncertainty in the correlation and characterizes overall jet behavior on a rather limited parameter. For the data presented here, the overall penetration is defined by the elevation of the first point above the injection centerline that has a fuel mass fraction less than 0.0007^3, although it should be noted that the same trends were observed in this data for mass fraction contours of 0.003 and 0.010. Within these limitations, the rate of overall penetration of the jet from the wedge-shaped injector is seen to be 42% greater than the rate of overall penetration of the jet from the circular injector.

Core penetration is based on the location of the local maximum, which eliminates the signal-to-noise concerns associated with overall penetration. However, for bifurcated cores, with low mixing occurring in the boundary layer, the local maximum will, at a sufficient distance downstream, be found in this near-wall region. The penetration may then actually become negative and the associated decay of local maximum concentration become very small. Since mass fluxes in the near-wall region will be low because of boundary-layer development, both core penetration and maximum concentration decay may not be representative of the overall mixing beyond the point where the local maximum is located in some secondary, near-wall core region. To account for this, comparisons between the two injection schemes are based primarily on the penetration of the local maximum in the main core region as seen in the contour plots. The jet from the circular injector split into two core regions as described, one that remained in the boundary layer and a second that penetrated into the freestream. The jet from the wedge-shaped injector did not separate as quickly and the main core penetrated into the freestream 64% farther than the main core of the jet from the circular injector. The rate of change of the core center penetration from the first axial station to the third axial station for the wedge-shaped injector was 89% greater than that of the circular injector.

Another type of penetration is defined by the location of the centroid of the lean limit cross-sectional area. Since this is associated with the jet cross section, which will continue to increase independently of any core divisions or reduced near-wall mixing, less ambiguity is associated with the interpretation of this penetration parameter. The choice of the hydrogen–air stoichiometric lean deflagration limit (at STP) is rather arbitrary as a boundary for identifying the jet cross section, but is believed to adequately represent the spread of the jet. Other contour lines may be more appropriate for other mixing applications. As the centroid penetrates farther into the freestream, more fuel jet surface area is exposed, enhancing mixing and combustion. The rate of penetration of the centroid for the jet from the wedge-shaped injector is 31% greater than the rate of centroid penetration for the jet from the circular injector. Also, the centroid for the jet from the wedge-shaped injector shows more penetration than the centroid for the jet from the circular injector at all three axial stations.

Since a single, normal jet has a three-dimensional flowfield, a measurement of the lateral spreading of the jet also provides a basis for mixing comparison. Lateral (or radial) expansion provides a greater jet surface area that can lead to faster mixing with the freestream. The growth of a defined cross-sectional area of a jet is an indication of overall expansion, not simply the penetration into the mean flow. The cross-sectional area used in this analysis is defined to be the area of the jet within the lean limit for homogeneous hydrogen–air deflagration. The rate of growth of this area for the jet from the wedge-shaped injector is 63% greater than the rate of area growth for the jet from the circular injector.

Considering the analyses in total, injection from the wedge-shaped injector shows a considerable improvement relative to circular hole injection. In addition, the essential elimination of the upstream separation zone should provide substantial reductions in heat transfer to the injection surface.

Conclusions

Sonic, normal injection into a Mach 3 freestream was investigated. Injection was through a circular wall orifice, which served as a baseline for comparison, and a wedge-shaped orifice. Based on surface oil-flow patterns, the upstream sepa-

ration zone present with circular orifice injection is absent with wedge-shaped orifice injection. This is expected to reduce thermal loading to the wall in this region. Additionally, the jet from the wedge-shaped injector shows greater penetration into the freestream and better mixing as evidenced by faster expansion of the jet cross section. As a fuel injection scheme for scramjet combustors, wedge-shaped wall injectors should provide generally better performance than circular injectors.

References

[1]Thomas, R. H., Schetz, J. A., and Billig, F. S., "Gaseous Injection in High Speed Flow," 9th International Symposium on Air Breathing Engines, Athens, Greece, Sept. 1989.

[2]Bogdanoff, D. W., "Advanced Injection and Mixing Techniques for Scramjet Combustion," *Journal of Propulsion and Power*, Vol. 10, No. 2, 1994, pp. 183–190.

[3]Rogers, R. C., "A Study of the Mixing of Hydrogen Injected Normal to a Supersonic Airstream," NASA TN L-7386, Sept. 1971.

[4]Rogers, R. C., "Mixing of Hydrogen Injected from Multiple Injectors Normal to a Supersonic Airstream," NASA TN L-7896, Sept. 1971.

[5]McClinton, C. R., "The Effect of Injection Angle on the Interaction Between Sonic Secondary Jets and a Supersonic Free Stream," NASA TN L-8125, Feb. 1972.

[6]Mays, R. B., "Experimental Investigation of Sonic Helium Injection at a Low Downstream Angle into Supersonic Flow," M.S. Thesis, Virginia Polytechnic Inst. and State Univ., Blacksburg, VA, June 1990.

[7]Schetz, J. A., and Billig, F. S., "Penetration of Gaseous Jets Injected into a Supersonic Stream," *Journal of Spacecraft and Rockets*, Vol. 3, No. 11, 1966, pp. 1658–1664.

[8]Billig, F. S., Orth, R. C., and Lasky, M., "A Unified Analysis of Gaseous Jet Penetration," *AIAA Journal*, Vol. 9, No. 6, 1971, pp. 1048–1058.

[9]Bussing, T. R. A., and Lidstone, G. L., "A Model for 3-D Sonic/Supersonic Transverse Fuel Injection into a Supersonic Air Stream," AIAA Paper 89-0460, Jan. 1989.

[10]Warfield, M. J., "Calculation of Supersonic Interacting Jet Flows," AIAA Paper 89-0666, Jan. 1989.

[11]Yu, S., and Shuen, J., "Three-Dimensional Simulation of an Underexpanded Jet Interacting with a Supersonic Cross Flow," AIAA Paper 88-3181, July 1988.

[12]Heister, S., and Karagozian, A., "The Gaseous Jet in Supersonic Crossflow," AIAA Paper 89-2547, July 1989.

[13]Masyakin, N. E., and Polyanskii, M. N., "On the Possibility of Blowing a Gas Jet into a Supersonic Flow Without Formation of a Three-Dimensional Boundary-Layer Separation Zone," *Izvestiya Akademii Nauk SSSR, Mekhanika Zhidkosti i Gaza*, No. 3, 1979, pp. 162–165.

[14]Kwok, F. T., Andrew, P. L., Ng, W. F., and Schetz, J. A., "Experimental Investigation of a Supersonic Shear Layer with Slot Injection of Helium," AIAA Paper 90-0093, Jan. 1990.

[15]Schetz, J. A., "Interaction Shock Shape for Transverse Injection in Supersonic Flow," *Journal of Spacecraft and Rockets*, Vol. 7, No. 2, 1970, pp. 143–148.

[16]Ng, W. F., Kwok, F. T., and Ninnemann, T. A., "A Concentration Probe for the Study of Mixing in Supersonic Shear Flows," AIAA Paper 89-2459, July 1989.